Journal of Biomedical Optics

SPIEDigitalLibrary.org/jbo

Imaging of biological tissues with pixel-level analysis of second-order susceptibility

Po-Sheng Hu
Ara Ghazaryan
Vladimir Hovhannisyan
Shean-Jen Chen
Yang-Fang Chen
Chang-Seok Kim
Tsung-Hua Tsai
Chen-Yuan Dong

SPIE

Imaging of biological tissues with pixel-level analysis of second-order susceptibility

Po-Sheng Hu,[b*] Ara Ghazaryan,[a*] Vladimir Hovhannisyan,[a] Shean-Jen Chen,[b] Yang-Fang Chen,[a] Chang-Seok Kim,[c] Tsung-Hua Tsai,[d] and Chen-Yuan Dong[a,c,e]
[a]National Taiwan University, Department of Physics, Taipei 106, Taiwan
[b]National Cheng-Kung University, Department of Engineering Sciences, Tainan, Taiwan
[c]Pusan National University, Department of Cogno-Mechatronics Engineering, Busan, Republic of Korea
[d]Far Eastern Memorial Hospital, Department of Dermatology, New Taipei City 220, Taiwan
[e]National Taiwan University, Center of Quantum Science and Engineering, Taipei 106, Taiwan

Abstract. We discuss the recent advances in the development and applications of second-order susceptibility as a contrast mechanism in optical microscopy for biological tissues. We review nonlinear optical methods and approaches for differentiation of tissue structures and discrimination of normal and pathological skin tissues, which have been demonstrated for the potential use in clinical diagnosis. In addition, the potential of second-order susceptibility imaging, encompassing applications in differentiating various types of collagen molecules for clinical diagnosis, is demonstrated. Finally, we discuss future development and application of this technique.
 [DOI: 10.1117/1.JBO.18.3.031102]

Keywords: second-order susceptibility; second harmonic generation; collagen; polarization-resolved microscopy.

Paper 12265VSS received Apr. 30, 2012; revised manuscript received Jul. 19, 2012; accepted for publication Jul. 20, 2012; published online Nov. 22, 2012.

1 Introduction

Light is a powerful tool for visualization and analysis of biological systems. However, the use of linear optical methods in biological studies has often had limited effectiveness. To be specific, in one-photon fluorescence microscopy, specimen photodamage, low signal-to-noise ratio caused by intrinsic scattering, and diffraction-limited resolution have constrained the range of biological problems that can be studied.[1,2] To overcome some of these issues, label-free imaging modalities that have distinct advantages in tissue imaging, such as increased imaging depths, were developed. The inherent drawbacks of conventional single-photon fluorescence microscopy have spurred improvement of instrumentation for biomedical diagnostics and therapeutics.[3–6] While confocal fluorescence microscopy provides axially discriminated sectioning of biological tissues, issues associated with specimen photodamage and the lack of enhanced imaging depths were alleviated by the application of near-infrared (NIR), ultrafast, femtosecond (*fs*) lasers. The reduced tissue absorption and photochemical action of NIR light allows greater imaging depths to be achieved and provides additional experimental capability by the use of nonlinear optical processes. Specifically, *fs*, NIR laser-induced nonlinear optical processes have proven viable imaging techniques for extracting contrast-specific signature of biological structures, such as molecular arrays of myosin, collagen, and lipid, allowing investigation of tissue structure and its organization as well as physiopathology of tissues at the cellular and molecular levels.[7–9] Since nonlinear optical processes can be registered with excitation intensity in the range of 10^6 to 10^8 W/cm^2,[10,11] such stringent requirements for photon flux limit excitation as well as the fluorescent signal collection to the focal volume and provides corresponding lateral and axial resolutions of around 220 and 520 nm, respectively, when focusing a 900-nm laser beam with a 1.2 numerical aperture objective lens.[12] To further improve contrast and sensitivity, laser-scanning multiphoton excitation fluorescence microscopy (LS-MPFM) has been combined with other optical modalities such as life-time imaging[13] and phase-contrast microscopy.[14]

Although MPFM enables *in vivo* live-animal modeling as well as clinical trials and yields a great wealth of insights into intricate structures, dynamic events, and interactive functions with significantly reduced photodamage, a majority of applications still require excitation of fluorescent species such as dye molecules, fluorescent nanocrystals, and beads.[15,16] Unlike multiphoton fluorescence excitation, which requires molecular electronic transition, second harmonic generation (SHG) involves a virtual interaction that converts two photons into a frequency-doubled photon with equivalent energy. The use of SHG is a complementary contrast mechanism for tissue imaging, and it has proven effective in imaging noncentrosymmetric biological structures such as arrays of collagen molecules.[17–19]

Moreover, development of SHG intensity-based techniques, such as integration with fluorescence lifetime imaging[20] and polarization-resolved SHG microscopy,[21] has evolved into versatile imaging systems. In an effort to elucidate morphological changes of biological tissues and their associated functions, induced second harmonic radiation in response to polarized laser beams has emerged as a useful modality.[22] Stoller et al. demonstrated for the first time pixel-level second-order susceptibility tensor $\chi^{(2)}$-based SHG imaging on the rat tendon, porcine cornea, and bovine tendon fascia with automated rotation of the linear polarization of the laser and a lock-in amplifier for SHG

*These authors contributed equally to this work.

Address all correspondence to: Tsung-Hua Tsai, Far Eastern Memorial Hospital, Department of Dermatology, New Taipei City, 220 Taiwan. E-mail: tsaitsunghua@yahoo.com.tw, or Chen-Yuan Dong, National Taiwan University, Department of Physics, Taipei 106, Taiwan. Tel: 886233665515; E-mail: cydong@phys.ntu.edu.tw.

signal registration, and they successfully revealed structural orientation mapping of the collagen fibril.[23] As an additional contrast parameter for imaging purposes, $\chi^{(2)}$ has also been used for differentiating biological structures and imaging of pathological tissues.[24,25] Additionally, pixel-resolved $\chi^{(2)}$ has been utilized as a quantitative imaging tool for characterizing axonemes obtained from sea urchin sperm and for identifying SHG sources in primary cortex neurons and amylopectin in starch. Other relevant techniques, such as spectral moment invariants analysis of polarization-modulated SHG images, have been implemented for quantifying textures of tissue and their disorders.[26] In this work, we focus on the review of second-order susceptibility microscopy (SOSM) along with pixel-level analysis for tissue imaging. In the context of this review, both the principles and technical basis of SOSM are described, followed by a discussion of applications of SOSM in imaging of normal and pathological tissues. We conclude with future prospects and potential in clinical diagnostics.

2 Background of Second Harmonic Generation

2.1 *Basis of SHG Origin in Biological Media*

Second-order nonlinear polarization of dielectric material effectively occurs when electromagnetic radiation with an oscillating electric field strength greater than 10^5 W/cm^2 interacts with noncentrosymmetric media.[27] In general, electromagnetic radiation-induced polarization of material system can be expressed as

$$P_i(\omega) = \chi_{ij}^{(1)} E_j(\omega) + \chi_{ijk}^{(2)} E_j(\omega) E_k(\omega) + \chi_{ijkl}^{(3)} E_j(\omega) E_k(\omega) E_l(\omega) + \ldots, \quad (1)$$

where $\chi^{(1)}$, $\chi^{(2)}$, and $\chi^{(3)}$ are, respectively, first-, second-, and third-order susceptibilities, E is the strength of electric field, and ω is the frequency. The nonlinear nature of SHG radiation sets a strict requirement for the medium to be noncentrosymmetric.[28] SHG was detected in quartz crystal shortly after the invention of a pulsed ruby laser operating at 694 nm.[27] Since then, the use of highly intense pulses has brought unprecedented advances in areas such as biological and biomedical sciences. The first observation of SHG stemming from biological tissues dates back in 1971, when collagen-rich Achilles tendons, scleras, and corneas of rabbits and dogs rendered a narrowband emission at 347 nm with irradiation of a Q-switched ruby laser at a wavelength of 694 nm.[29] The scheme of scanning SHG microscopy for investigating nonlinear crystals was proposed and built in 1978, which set an important stage for its use in biological applications.[30] A number of biological materials, such as cartilage, tendons, myosin-rich striated muscle, crystallized microtubules of mitotic spindles, and plant chloroplast, have been found capable of generating the second harmonic signal.[31–36] Thus, the identification of SHG sources within biological media is of primary importance for its further application in studies of the characteristics of biological organisms. The basis of SHG can be explained from molecular hyperpolarizability β,[19] given as

$$\beta \sim \frac{3e^2}{2h^3} \frac{\omega_{ge} f_{ge} \Delta\mu_{ge}}{[\omega_{ge}^2 - \omega^2][\omega_{ge}^2 - 4\omega^2]}. \quad (2)$$

This formula accounts for the transition frequency ω_{ge}, the oscillator strength derived from an integral of absorption spectrum f_{ge}, the and change in dipole moment $\Delta\mu_{ge}$ of ground and excited states, in which e is the constant of electric charge and h is the Planck constant. Macroscopic second-order susceptibility $\chi^{(2)}$ is proportionally related to β,[19] as shown in the following expression:

$$\chi^{(2)} = N_s \langle \beta \rangle, \quad (3)$$

where N_s is the spatial density of molecules and the bracketed β denotes the orientation average of molecules, indicating the requirement of a noncentrosymmetric environment for optical second-order nonlinear process. Experimentally, second harmonic radiation can be induced by the impingement of *fs* pulses upon nonlinear media and is scaled[19] as

$$\mathrm{SHG}_{\mathrm{sig}} \propto \rho^2 \tau (\chi^{(2)})^2, \quad (4)$$

where ρ and τ are the excitation intensity and pulse duration of the *fs* laser pulse, respectively. Integration of Eqs. (3) and (4) shows that SHG intensity is quadratically proportional to concentration of molecules which act as individual dipole antenna. The SHG signal rendered from the use of high-intensity *fs* pulses upon nonlinear media have brought advances in the diagnostics of tissue structure rich in collagen and myosin.[8,21,28]

Since 1986, the application of scanning second harmonic microscopy has revealed polarization of filamentous, columnar structures of collagen fibril in native rat tail tendons, which exhibit the directionality that permeate the tendon cross-section.[37] Since then, SHG microscopy, a complementary, structure-sensitive tool to MPFM, has found enormous usefulness in optical tissue biopsy and reconstruction of intact structure of mammalian tissues, as well as in the study of local cellular membrane morphology and its dynamics, which were previously unattainable with conventional histology.[38–40] A mixture of type I and V collagen emulating the state of human breast cancer has been quantifiably diagnosed with SHG intensity measurement, which deceases in parallel with an increase in the content of Col V; mixture with lower Col V is also characterized by longer fibers and a higher emission ratio of Forward SHG to Backward SHG FSHG/BSHG.[41] A similar investigation on breast cancer using SHG microscopy also clarified the relationship between collagen density and carcinogenesis. In that investigation, three tumor-associated collagen signatures were observed and defined based on density, shape, and orientation of collagen fibers, which may provide novel markers for locating and characterizing tumors.[42] Another study concerning ovarian cancer used the integration of three-dimensional (3D) SHG intensity and bulk optical measurements, as well as Monte Carlo simulations, to investigate the remodeling of structure of ovarian extracellular matrix in a cancerous state. This study revealed lower cell density, denser collagen, and higher regularity at both fibril and fiber levels in malignant tissues.[43] When used in combination with Monte Carlo simulations or an assessment computation algorithm, SHG microscopy is also capable of identifying the diseased state osteogenesis imperfect, as well as discriminating different collagen types in kidney tissue.[44,45]

Furthermore, manual and acoustooptical polarization-swept *fs* light sources can help determine the detailed content within the subsurface of tissues.[46,47] Polarization signature of tissues, such as skin and cartilage, has added an additional contrast mechanism to intensity-based investigation and has allowed differentiation of normal and morphologically variant tissues.[9,28,48] For instance, variations of collagen fiber organization and orientation in normal cartilage were revealed and differentiated from degenerated cartilage using polarization-sensitive SHG and ratio

of intensities of two orthogonally polarization-resolved SHG signals.[49] Previously, using polarization-resolved SHG microscopy, Nucciotti et al. assigned a unique value of polarization anisotropy to each physiological/biochemical state of myosin structural conformation, which helped discriminate between attached and detached myosin heads in a contracting intact fiber.[50]

Polarization-sensitive SHG microscopy has been used to investigate structure and molecular composition of tissues such as corneal stroma and skeletal muscle tissues.[51,52] In addition, specific polarization properties of collagen and myosin were distinguished using polarization-selective SHG intensities and their ratios.[53,54] Researchers have applied polarization-sensitive SHG measurements to enable second-order susceptibility tensor-based quantification for numerical analysis of biological tissues. To show this quantification approach, Fig. 1 illustrates the relationship of a linearly polarized laser beam with a propagation vector along the y-axis and the orientation of collagen fibril (Φ_F), together with the direction of laser polarization (Φ_L), which are defined as relative angles with respect to the vertical z-axis on the plane of the xz-coordinate system. The relative angular difference $\varphi = \Phi_F - \Phi_L$ is used in numerical analysis.[55] Under the assumption of cylindrical symmetry, elements of second-harmonic susceptibility tensor reduce to four independent elements.[56] With the angular definition of φ, the induced SHG intensity can be expressed[55] as

$$P_x = (d_{15}\ \sin\ 2\varphi)E^2 \quad P_z = (d_{31}\sin^2\varphi + d_{33}\cos^2\varphi)E^2, \tag{5}$$

where the x and z components of induced SHG intensities are functions of φ, E is the amplitude of the electric field, and the contracted notations $d_{15} = \chi^{(2)}_{xzx}/2$, $d_{31} = \chi^{(2)}_{zxx}/2$, and $d_{33} = \chi^{(2)}_{zzz}/2$ are denoted for the description of second-order susceptibility tensor elements. In addition, φ is an angle between the principle axis and the polarization direction of laser radiation, since fiber orientation was previously shown to be equivalent to the principle axis of second-order susceptibility tensors.[8] As a result, the overall polarization-sensitive SHG intensity can be written as a combination of individual components[55] shown below:

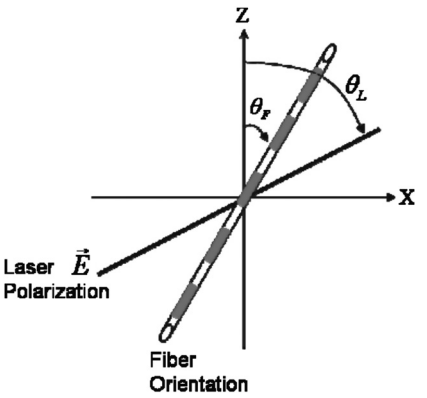

Fig. 1 Illustration of laser polarization and fiber orientation in a coordination system. Φ_F is the angle of fiber orientation relative to the z-axis, and (Φ_L) is the polarization angle of the electric field vector of an incoming laser with a propagation vector along the y-axis.[55]

$$I \sim P_x^2 + P_z^2 \sim \{(\sin\ 2\varphi)^2 + (\sin^2\varphi + \cos^2\varphi^2)^2\}E^4. \tag{6}$$

Equation (6) can be used to fit the SHG intensity as a function of φ. As a result, χ_{xzx}/χ_{zxx}, χ_{zzz}/χ_{zxx}, fiber orientation Φ_F, and the overall proportionality constant can be determined. These parameters would then allow the quantitative characterization of noncentrosymmetric biological tissues. For instance, averaged ratios of $\chi_{zzz}/\chi_{zxx} = 1.40\mp0.04$ and $\chi_{xzx}/\chi_{zxx} = 0.53\mp0.10$ were previously determined as a footprint indicating type I collagen of rat tail tendon;[57] validity of these ratios is discussed from experimental aspects in the following sections.

3 Applications in Clinics and Basic Sciences

3.1 *Clinical Dermatology*

Skin, as the outermost protective organ, separates internal soft tissue from external environment and biochemically plays a major role in immunoregulation and maintenance of physiological homeostasis.[58] The composition of skin can be divided mainly into three sections: epidermis, dermis, and hypodermis. The basal layer, the deepest layer of epidermis, is essentially composed of basal and other cells and is responsible for the synthesis and division of newly formed keratinocytes, which migrate superficially and form spinous and granular layers in the ascending order of cellular maturity with corneum, a lamina of anucleate cells, residing in the outermost layer. The dermis lies immediately underneath the epidermis and consists of an extracellular matrix containing collagen and elastic fibers. Depending on sections of superficial skin, the thickness of the epidermis and dermis range from 50 to 1,500 μm and 100 to 500 μm, respectively.[52] The subcutaneous depth ranges are measurable using optical imaging modalities and have proven to be readily accessible for diagnostic purposes.[59] Dermatological science has made significant progress in parallel with advancements in optical microscopy, which have helped resolve cellular and molecular constituents of subcutaneous tissues in applications such as *in vivo* monitoring of lesions, presurgical illustration of basal cell carcinoma,[60] and noninvasive assessment of the skin's microvascular function[61] and related dermatological diseases such as atopic dermatitis.[62] While confocal fluorescence microscopy can visualize cellular components of the stratum corneum and discriminate the junction of the dermis and epidermis, upon reflection, multiphoton microscopy capable of probing depths greater than a few hundred microns is inherently more suitable for interrogating physical and biochemical properties of deep tissue.[63] At the junction between the dermis and epidermis, the laminar structure of epidermal cells, melanin, elastin, and collagen fibers was observed instantaneously with a combined imaging modality of spectra of autofluorescence (AF) and SHG microscopy.[64] A combination of AF and SHG measurements has also proven invaluable in assessing characteristics of skin aging and pathological conditions *in vivo*.[65] In addition, early detection of alterations in the physical and biochemical properties of subcutaneous cellular constituents and structural lamination within human skin biopsy has been demonstrated utilizing an imaging system combining OCT and MPM.[66] Change in collagenous structure-induced SHG response has helped discriminate normal derma from basal cell carcinoma and has allowed *in vivo*, guidance for basal cell carcinoma removal.[67] Likewise, merits of second-order susceptibility imaging lie not only in assessment of tissues

with polarization-dependent intensities, but also in providing quantification at a pixel-by-pixel level that serves as a metric for differentiating types, composition, and physiopathological states of tissues. Pixel-level analysis of polarization-dependent SHG measurements has successfully revealed structures of different muscle cells of living Caenorhabditis elegans (C. Elegans) nematodes, as well as differentiated fibrillar collagen and skeletal muscle in mammalian tissues.[68,69] Additionally, development on 1D Fourier and the gray-level co-occurrence matrix analyzes of polarization-sensitive SHG measurements have helped enhance the contrast of images and increase imaging speed nearly five-fold, respectively.[70,71]

In our study, molecular origins of SHG sources were quantitatively distinguished in collagen-rich human dermis and the muscle-tendon junction of chicken wings rich in both collagen and myosin using second-order susceptibility imaging.[24]

Before obtaining second-order susceptibility tensors from human dermis, SHG tensors analysis was performed on the muscle-tendon junction, making sure that results of the imaging technique were valid and capable of discriminating between different SHG origins.

Figure 2 shows single-pixel-resolved mapping of the second-order susceptibility tensor ratios χ_{zzz}/χ_{zxx} and χ_{xzx}/χ_{zxx} derived from polarization-dependent SHG signal by imaging the muscle-tendon junction of chicken wings. The SHG intensity value of each pixel was taken as an average with eight surrounding pixels for enhancing visual impression by smoothing out color-code transition between pixels before image processing, which does not signify any quantitative manipulation to the original data. The tomography of the tensor ratios χ_{zzz}/χ_{zxx} and χ_{xzx}/χ_{zxx} indicates morphological difference between muscle and tendon; tendon is a much stronger SHG emitter than muscle, so image contrast revealed the boundary of the junction. The polarization-dependent SHG intensity at 21 different excitation polarization angles over an angular range of 0 deg to 180 deg were measured to determine χ_{zzz}/χ_{zxx}, χ_{xzx}/χ_{zxx}, fiber angle Φ_F, and the proportionality constant by least-square-fitting of Eq. (6) and construct image maps of χ_{zzz}/χ_{zxx} and χ_{xzx}/χ_{zxx}, which are illustrated in Fig. 2(a) and 2(b), respectively. As can be seen from Fig. 2(a), χ_{zzz}/χ_{zxx} clearly elucidates the contrast between muscle and tendon, whereas such clear distinction is not presented in tomography of χ_{xzx}/χ_{zxx}. Figure 2(e) delineates the variation of normalized SHG intensity as a function of polarization angle relative to fiber angle for pixels 1 and 2 marked on Fig. 2(a), and error bars were taken over three repeated images. The respective peak values of χ_{zzz}/χ_{zxx} are 1.04 ± 0.08 (dashed arrow) and 1.34 ± 0.07 (solid arrow) for the muscle and tendon, as shown in Fig. 2(c), which demonstrated the effectiveness of SOSM as an imaging contrast mechanism for differentiating the SHG origin of muscle and tendon. Also, note that the dual-peak profile in the histogram of Fig. 2(c) illustrates clear differences of χ_{zzz}/χ_{zxx} for muscle and tendon. On the other hand, as with previous results for rat tail tendons, χ_{xzx}/χ_{zxx}, shown in Fig. 2(d), is not close to 1 and does not show such two-peak distinction. Since Eq. (6) was derived under the assumptions of Kleinman and cylindrical symmetries, which reduce the number of second-order susceptibility tensors, the ratio of χ_{xzx}/χ_{zxx} is theoretically set to 1 when assumptions are applied to lossless media with the excitation frequencies being far away from absorption frequencies of the media.[72] Although the validity of these assumptions was verified by Stoller et al. for the reason that the first electronic transition in collagen (at 310 nm) is far away from the SHG wavelength at 400 nm, other experimental groups have found their results of χ_{xzx}/χ_{zxx} slightly deviated from theory.[23] Both Chu et al. and Plotnikov et al. have made the similar argument that their laser excitation and SHG frequencies were not too far away from the resonant frequency of muscle, which may attribute to a slight deviation from Kleinman symmetry.[9,73] Under the context of the assumption discussed here, the affinity of our SHG wavelength (390 nm) to the resonant wavelength of collagen at 350 to 380 nm may well contribute to a slight deviation from Kleinman

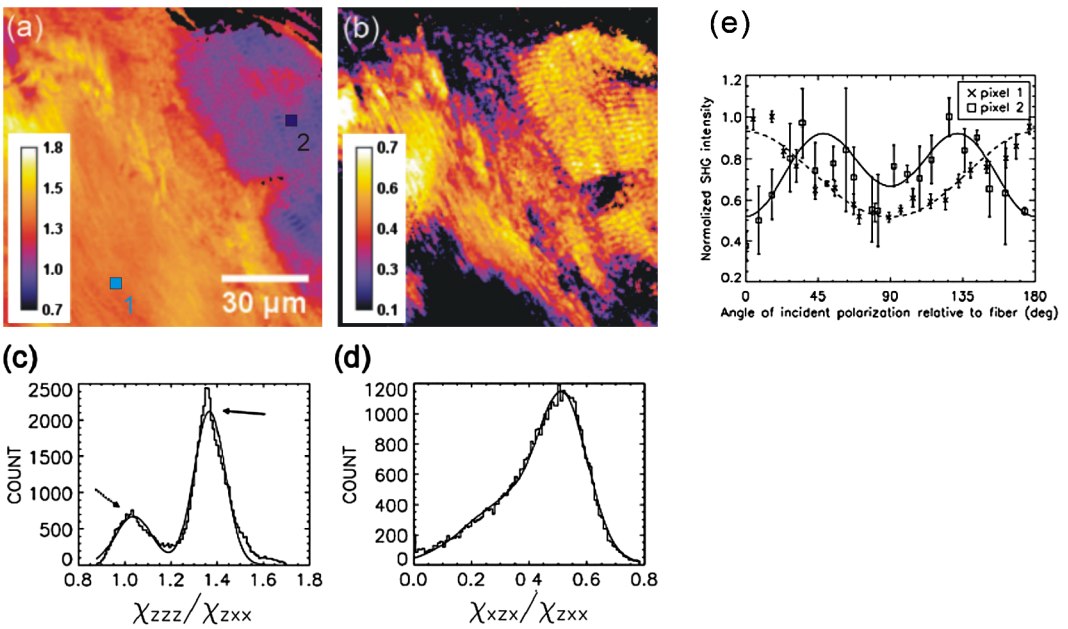

Fig. 2 Quantitative analysis of second-order susceptibility tensor ratios on the muscle-tendon junction a of chicken wing. Tomography of (a) χ_{zzz}/χ_{zxx} and (b) χ_{xzx}/χ_{zxx} are illustrated along with histograms of occurrence count for (c) χ_{zzz}/χ_{zxx} and (d) χ_{xzx}/χ_{zxx}. Variation of SHG intensity as a function of relative angle between fiber direction and laser polarization for pixel locations 1 and 2 are shown in (a).[24]

symmetry. In addition, a wavelength of 900 nm has been used by other experimental groups to excite myosin molecules of mice leg muscles, as well as mice tail tendon fascia and muscle fascia, which render an SHG emission of 450 nm and thus confirm the contribution of SHG resonance to the deviation from Kleinman symmetry.[54,74] Another possible explanation for such a ratio deviation is the chirality of collagen, which is known to enhance SHG radiation and thus may vary the χ ratio contribution accordingly.[75,76]

Following the same analytic procedures, SOSM was used to examine human dermis. Figure 3 shows a second-order susceptibility analysis of polarization-sensitive SHG intensity images. SHG intensity images shown in Fig. 3(a), 3(b), and 3(c) delineate the single-pixel-resolved tomography of polarization-dependent SHG intensity, χ_{zzz}/χ_{zxx}, and χ_{xzx}/χ_{zxx}, respectively. The results of immunohistology revealed collagen I as the main component of fibril bundles in human dermis, which is consistent with analysis of second-order susceptibility within the encircled region of Fig. 3(b); the averaged χ_{zzz}/χ_{zxx} was determined to be 1.34 ± 0.07. The histogram of χ_{zzz}/χ_{zxx} is presented in Fig. 3(d), where the first peak value of 1.23 ± 0.09 corresponds to collagen type I, while the second peak value of 0.92 ± 0.08 could be attributed to collagen type III, another major constituent of the dermis. Furthermore, as reported previously, χ_{zzz}/χ_{zxx} was used for differentiating human dermis under different pathological conditions: keloid, morphea, and dermal elastolysis, which were characterized by peak χ_{zzz}/χ_{zxx} values of 1.67 ± 0.29, 1.79 ± 0.30, and 1.75 ± 0.31, respectively.[25]

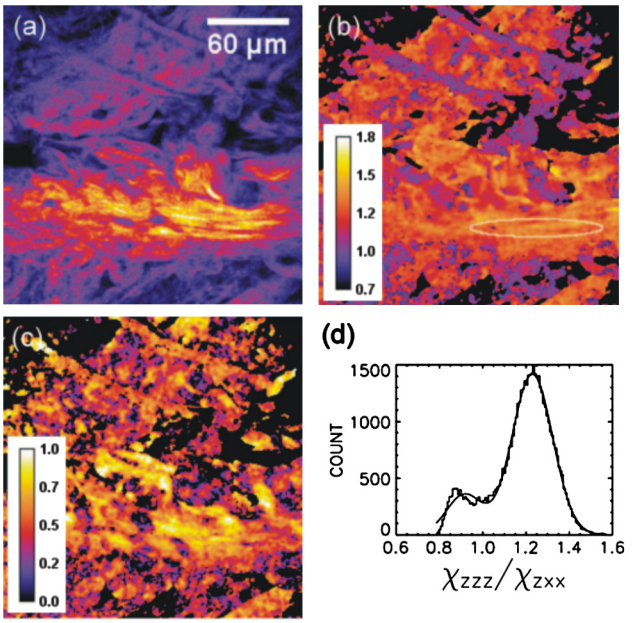

Fig. 3 Second-order susceptibility analysis of SHG images of human dermis. (a) An SHG intensity image. (b) Single-pixel-resolved mapping of χ_{zzz}/χ_{zxx}. (c) Single-pixel-resolved mapping of χ_{xzx}/χ_{zxx}. (d) Occurrence count for χ_{zzz}/χ_{zxx}.[24]

3.2 *Basic Studies and Tissue Engineering Applications*

Connective tissues of a variety of mammalian and amphibian species have been found to be made of different types of collagen.[77,78] Fibrillar collagen, such as type I, exhibits SHG radiation attributing to coherent effects of the high-density and quasicrystalline structure of collagen fibril, and it has been explored for intensity-based characterization of tissue properties. Specifically, through the use of polarization-sensitive SHG and MPF measurement, normal and degenerate equine articular cartilage were differentiated, and it was suggested that numerical models are required for quantification of depth-dependent polarization measurement.[49] In another study, unraveling endogenously hidden myosin-rich and collagen-rich tissues in amphibian and mammals was achieved.[79] Furthermore, polarization-sensitive SHG measurements were used to characterize the orientation angle of myosin in collagen I and collagen III.[77] Hyper-Raileigh scattering experiments were carried out, and peptide bonds were found to be the molecular origin of SHG in proteins.[80] Using sum-frequency generation vibrational spectroscopy, it was found that molecular SHG also originated from the methylene group associated with Fermi resonance between the fundamental symmetric stretch and the bonding overtone of methylene, and that carbonyl and peptide groups associated with the amide I band are the dominant SHG contributors.[81] Our study revealed that the molecular origin of collagen-rendered second-order susceptibility not only is attributed to the peptide groups in the backbone of the

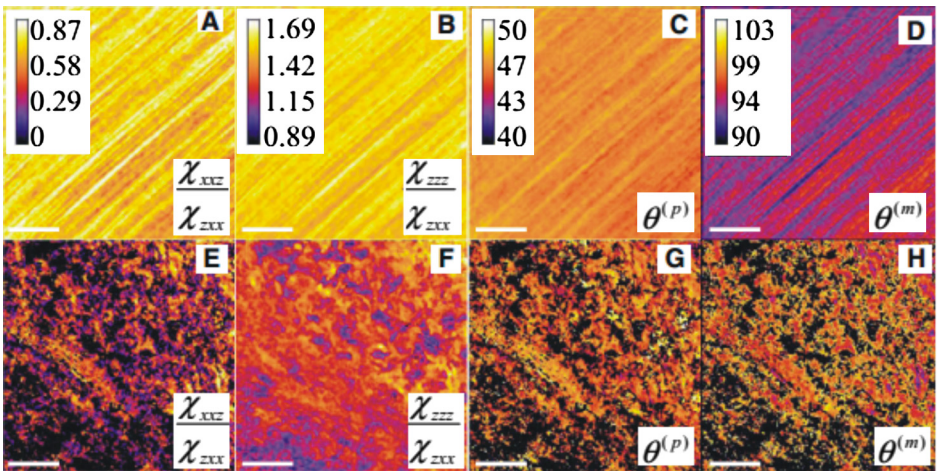

Fig. 4 An analysis of second-order susceptibility tensors with collagen I from rat tail tendons and collagen II from rat trachea cartilage. χ_{zzz}/χ_{zxx}, χ_{xzx}/χ_{zxx}, $\theta^{(p)}$, and $\theta^{(m)}$ for collagen I and II are shown on the top row (a-d) and the bottom row (e-h), respectively.[82]

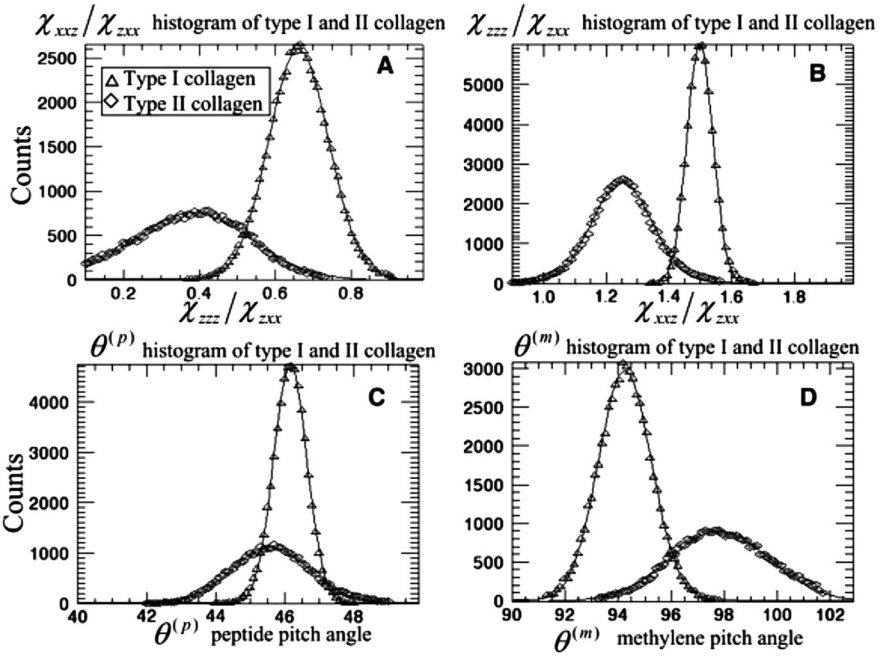

Fig. 5 An analysis of second-order susceptibility tensors. Occurrence-count histograms of (a) χ_{zzz}/χ_{zxx}, (b) χ_{xzx}/χ_{zxx}, (c) $\theta^{(p)}$, and (d) $\theta^{(m)}$ for type I and type II collagen, delineating comparison between these types of collagen.[82]

collagen α-helix but may also be attributed to the methylene groups in the pyrrolidine rings.[82] With this work, we demonstrated the visualization and differentiation of different SHG origins, namely, different types of collagen.

These results allow the construction of χ tensor ratio maps. A peptide pitch-angle $\theta^{(p)}$ of 45.82 ± 0.46 deg and a methylene pitch-angle $\theta^{(m)}$ of 94.80 ± 0.97 for collagen I from rat tail tendons were estimated, which comply with previous results of x-ray diffraction upon collagen-like peptide. Moreover, collagen II from rat trachea cartilage yielded similar results for $\theta^{(p)}$ of 45.75 ± 1.17 deg, whereas $\theta^{(m)}$ of 97.87 ± 1.79 deg was slightly different from that of collagen I. Figure 4 shows

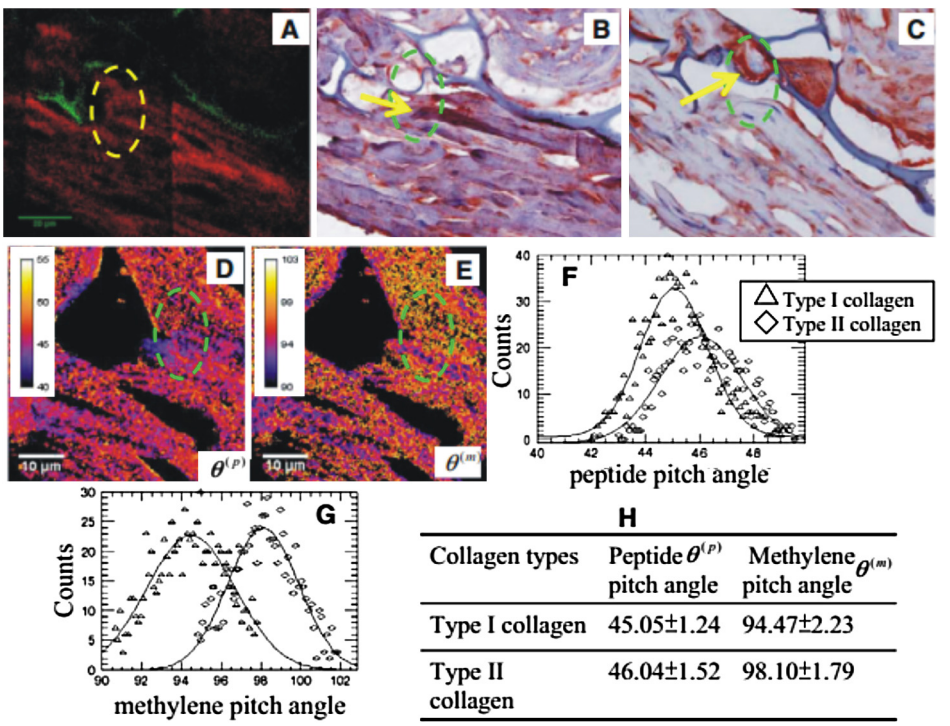

H

Collagen types	Peptide $\theta^{(p)}$ pitch angle	Methylene $\theta^{(m)}$ pitch angle
Type I collagen	45.05±1.24	94.47±2.23
Type II collagen	46.04±1.52	98.10±1.79

Fig. 6 An MPM image analysis on the selected region for identifying collagen type I and II in a sample of engineered cartilage. (a) The polarization-dependent MPM image. Immunochemical staining confirms the presence of (b) collagen type I and (c) collagen type II. Tomography of (d) $\theta^{(p)}$ and (e) $\theta^{(m)}$, along with color bars, illustrate the results of second-order susceptibility analysis and single-pixel-resolution of SOSM images. The encircled regions of (d) and (e) are analyzed for distribution of occurrence counts of (f) $\theta^{(p)}$ and (g) $\theta^{(m)}$, indicating characteristics of collagen type I and II. (h) The characteristics are tabulated in a table.[82]

tomographic images of χ_{zzz}/χ_{zxx}, χ_{xzx}/χ_{zxx}, $\theta^{(p)}$, and $\theta^{(m)}$ for type I and II collagens, with type I on the top row (a-d) and type II on the bottom (e-h). Likewise, the histogram of χ_{zzz}/χ_{zxx}, χ_{xzx}/χ_{zxx}, $\theta^{(p)}$, and $\theta^{(m)}$ for both type I and II collagens is shown in Fig. 5(a) to 5(d). These results demonstrate the capability of SOSM for identifying different molecular origins of SHG radiation.

SOSM imaging has also been used to probe engineered cartilage tissue containing both type I and II collagens; in contrast, native cartilage is mainly composed of type II.[57] The results of second-order susceptibility tensor analysis from a polarization-dependent SHG image are shown in Fig. 6(a). Immunochemical staining was performed to confirm the presence of collagen I and II, as shown in Fig. 6(b) and 6(c), respectively. Figure 6(d) and 6(e) are the corresponding images of peptide pitch-angle and mythelene pitch-angle. Second-order susceptibility tensor analysis, performed within the dashed encircled regions of Fig. 6(d) and 6(e) are presented, respectively, in Fig. 6(f) and 6(g), illustrating the histograms of peptide- and mythelene pitch-angles for type I and II collagens. These results are summarized in Fig. 6(h), which shows a table of numerical data for $\theta^{(p)}$ and $\theta^{(m)}$ characterizing type I and II collagens. Clearly, with these results, the validity of SOSM in identifying type I and II collagens in a mixture of engineered cartilage has been verified.

4 Discussion

The most recent application of polarization-resolved SHG imaging has helped determine orientation mapping of collagen fibril in cornea[83] and reveal three thermaldynamic stages in collagen denaturation.[84] Moreover, developmental efforts of 3D analysis have been carried out for biological structures, such as inherent crystallinity of amylopectin in starch grain, and orientation mapping for collagen fibril in mammalian tissues such as bovine legs, chicken legs, and chicken skin by extracting information from the elevation angle.[85,86] For thin tissue specimens, BSHG is attributed to the backscattering of FSHG, whereas in thick tissue, BSHG is less than 1% of FSHG, which yields more informative images than BSHG.[87,88] Based on the difference in coherence interaction lengths for FSHG and BSHG, selective SHG imaging has been demonstrated to discriminate collagen fibrils from muscle fibers by BSHG and FSHG imaging, respectively, which suggests the usefulness of backward and forward imaging for different applications.[89] As for biomedical imaging, BSHG imaging is a more suitable modality for practical purposes.

Despite the enormity of information being extracted using SHG imaging, several limitations, such as the turbid nature of tissue media, which causes strong backscattering, have dwindled its capability in determining authentic tissue structure, function, and dynamics.[90] Furthermore, SHG sources such as collagen are anisotropic in optical index refraction and thus render strong effects of birefringence, diattenuation, and polarization cross-talks as the imaging fathom gets deeper, which causes depolarization.[22,91,92] This must be taken into account in future work for obtaining information at depths greater than 20 μm. Several birefringence studies on tendons, cartilage, and other tissues such as dentine, dermis, and bones using BSHG imaging have confirmed depth-dependent variation of polarization sensitivity patterns, which limits the depth resolution of SOSM.[49]

In the current setting of experimental instrumentation, improvement is possible on several fronts to extend the functionality and versatility of biological experiments. One example is the speed of manually adjusted polarization, which can be replaced with an electrooptically automated polarization adjustable microscopic system to shorten the time of data acquisition and to keep samples at homeostasis better. So far, a majority of applications utilizing nonlinear microscopy have focused on skin, eyes, and oral cavities, which are readily accessible by optics. Nonlinear endoscopy has been developed and may be conducive for internal organ treatments, but it has not been demonstrated extensively in research and clinics like its microscopic counterpart. Another area where SHG microscopy can improve is the modulation of laser pulse duration, which is also not extensively investigated, perhaps due to the cost of instrumentation and the complexity of a nonlinear optic setup for manipulating pulse duration. By interrogating the impact of variation in pulse duration on human skin *in vivo*, Tromberg et al. found that the SHG signal is inversely proportional to the pulse duration in both forward and backward detection.[93] With additional development incorporating technologies such as efficiency enhancement of nonlinear processes through spectral pulse shaping-controlled polarization, as well as micro-electro mechanical system (MEMS)-based adaptive optics and microendoscopy, SOSM may find new applications in both clinical and basic research.[94]

5 Conclusion

Recent development of the use of second-order susceptibility analysis as an additional imaging tool has expanded the capabilities of SHG microscopy. Not only can it be applied to solving biomedical problems such as detection of pathological skin tissues, but this approach has also shown promise in basic studies and tissue engineering applications for collagen. Multiphoton imaging of biological media and their constituents has opened up a brand-new page in biomedical and basic science research. Specifically, label-free, nonlinear optical microscopy has found applications in both clinical and research communities, where, in addition to fluorescence imaging, SHG can be used as an image contrast mechanism for imaging of noncentrosymmetric biological tissues. In this study, the technical basis of SOSM has been described in the context of evolutionary development and related scientific experiments. The merits of SOSM, such as contrast enhancement, quantification, and differentiation of different types of tissues, were demonstrated.

Acknowledgments

We would like to acknowledge the support of the National Science Council (NSC 101-2112-M-002-003-MY3, NSC 99-2221-E-002-008-MY3, NSC 100-2314-B-418-009), National Health Research Institute (NHRI-EX10010041EI), Center of Quantum Science and Engineering (CQSE-10R80914), and National Taiwan University (NTU-101R70804). Partial support was provided by the World Class University (WCU) program of Korea.

References

1. F. Helmchen and W. Denk, "Deep tissue two-photon microscopy," *Nat. Methods* **2**(12), 932–940 (2005).
2. K. Svoboda and R. Yasuda, "Principles of two-photon excitation microscopy and its applications to neuroscience," *Neuron* **50**(6), 823–839 (2006).
3. R. S. Weinstein, "Innovations in medical imaging and virtual microscopy," *Hum. Pathol.* **36**(4), 317–319 (2005).

4. A. V. Loparev, A. V. Kretushev, and V. P. Tychinskii, "Coherent phase microscopy: a new method of identification of intracellular structures based on their optical and morphometric parameters," *Biofizika* **53**(2), 299–304 (2008).
5. A. Lewis et al., "Near-field scanning optical microscopy in cell biology," *Trends Cell. Biol.* **9**(2), 70–73 (1999).
6. B. W. Leslie et al., "Radial fibre proportions in human knee joint menisci—measurement by scanning optical microscopy," *Acta. Anat.* **163**(4), 212–217 (1998).
7. S. Ghose et al., "Rare earth cryptates for the investigation of molecular interactions *in vitro* and in living cells," *J. Alloy Compd.* **451**(1–2), 35–37 (2008).
8. C. Odin et al., "Collagen and myosin characterization by orientation field second harmonic microscopy," *Opt. Express* **16**(20), 16151–16165 (2008).
9. S. V. Plotnikov et al., "Characterization of the myosin-based source for second-harmonic generation from muscle sarcomeres," *Biophys. J.* **90**(2), 693–703 (2006).
10. P. T. C. So et al., "Two-photon excitation fluorescence microscopy," *Annu. Rev. Biomed. Eng.* **2**, 399–429 (2000).
11. W. Denk, J. H. Strickler, and W. W. Webb, "2-photon laser scanning fluorescence microscopy," *Science* **248**(4951), 73–76 (1990).
12. W. R. Zipfel, R. M. Williams, and W. W. Webb, "Nonlinear magic: multiphoton microscopy in the biosciences," *Nat. Biotechnol.* **21**(11), 1368–1376 (2003).
13. K. M. Hanson et al., "Two-photon fluorescence lifetime imaging of the skin stratum corneum pH gradient," *Biophys. J.* **83**(3), 1682–1690 (2002).
14. E. Shaffer et al., "Label-free second-harmonic phase imaging of biological specimen by digital holographic microscopy," *Opt. Lett.* **35**(24), 4102–4104 (2010).
15. G. S. Filonov et al., "Bright and stable near-infrared fluorescent protein for *in vivo* imaging," *Nat. Biotechnol.* **29**(8), 757–761 (2011).
16. M. D. Cahalan et al., "Two-photon tissue imaging: seeing the immune system in a fresh light," *Nat. Rev. Immunol.* **2**(11), 872–880 (2002).
17. A. Zoumi, A. Yeh, and B. J. Tromberg, "Imaging cells and extracellular matrix *in vivo* by using second-harmonic generation and two-photon excited fluorescence," *Proc. Natl. Acad. Sci. USA* **99**(17), 11014–11019 (2002).
18. W. R. Zipfel et al., "Live tissue intrinsic emission microscopy using multiphoton-excited native fluorescence and second harmonic generation," *Proc. Natl. Acad. Sci. USA* **100**(12), 7075–7080 (2003).
19. P. J. Campagnola and L. M. Loew, "Second-harmonic imaging microscopy for visualizing biomolecular arrays in cells, tissues and organisms," *Nat. Biotechnol.* **21**(11), 1356–1360 (2003).
20. S. Vesuna, R. Torres, and M. J. Levene, "Multiphoton fluorescence, second harmonic generation, and fluorescence lifetime imaging of whole cleared mouse organs," *J. Biomed. Opt.* **16**(10), 106009 (2011).
21. S. W. Chu et al., "Selective imaging in second-harmonic-generation microscopy by polarization manipulation," *Appl. Phys. Lett.* **91**(10), 103903 (2007).
22. S. Brasselet et al., "Influence of birefringence on polarization resolved nonlinear microscopy and collagen SHG structural imaging," *Opt. Express* **18**(14), 14859–14870 (2010).
23. P. Stoller et al., "Polarization-modulated second harmonic generation in collagen," *Biophys. J.* **82**(6), 3330–3342 (2002).
24. W. L. Chen et al., "Second harmonic generation chi tensor microscopy for tissue imaging," *Appl. Phys. Lett.* **94**(18), 183902 (2009).
25. P. J. Su et al., "Discrimination of collagen in normal and pathological skin dermis through second-order susceptibility microscopy," *Opt. Express* **17**(13), 11161–11171 (2009).
26. M. Wang, K. M. Reiser, and A. Knoesen, "Spectral moment invariant analysis of disorder in polarization-modulated second-harmonic-generation images obtained from collagen assemblies," *J. Opt. Soc. Am. A* **24**(11), 3573–3586 (2007).
27. P. A. Franken et al., "Generation of optical harmonics," *Phys. Rev. Lett.* **7**(4), 118–119 (1961).
28. P. J. Campagnola and C. Y. Dong, "Second harmonic generation microscopy: principles and applications to disease diagnosis," *Laser Photonics Rev.* **5**(1), 13–26 (2011).
29. S. Fine and W. P. Hansen, "Optical second harmonic generation in biological systems," *Appl. Opt.* **10**(10), 2350–2353 (1971).
30. J. N. Gannaway and C. J. R. Sheppard, "2nd-harmonic imaging in scanning optical microscope," *Opt. Quant. Electron.* **10**(5), 435–439 (1978).
31. M. Rehberg et al., "Label-free 3D visualization of cellular and tissue structures in intact muscle with second and third harmonic generation microscopy," *PLoS One* **6**(11), e28237 (2011).
32. E. Ralston et al., "Detection and imaging of non-contractile inclusions and sarcomeric anomalies in skeletal muscle by second harmonic generation combined with two-photon excited fluorescence," *J. Struct. Biol.* **162**(3), 500–508 (2008).
33. G. Cox, N. Moreno, and J. Feijo, "Second-harmonic imaging of plant polysaccharides," *J. Biomed. Opt.* **10**(2), 024013 (2005).
34. M. Rivard et al., "The structural origin of second harmonic generation in fascia," *Biomed. Opt. Express* **2**(1), 26–36 (2011).
35. A. H. Reshak, V. Sarafis, and R. Heintzmann, "Second harmonic imaging of chloroplasts using the two-photon laser scanning microscope," *Micron* **40**(3), 378–385 (2009).
36. S. W. Chu et al., "*In vivo* developmental biology study using noninvasive multi-harmonic generation microscopy," *Opt. Express* **11**(23), 3093–3099 (2003).
37. I. Freund, M. Deutsch, and A. Sprecher, "Connective-tissue polarity—optical 2nd-harmonic microscopy, crossed-beam summation, and small-angle scattering in rat-tail tendon," *Biophys. J.* **50**(4), 693–712 (1986).
38. Y. Guo et al., "Second-harmonic tomography of tissues," *Opt. Lett.* **22**(17), 1323–1325 (1997).
39. P. J. Campagnola et al., "Second-harmonic imaging microscopy of living cells," *J. Biomed. Opt.* **6**(3), 277–286 (2001).
40. L. Moreaux et al., "Membrane imaging by simultaneous second-harmonic generation and two-photon microscopy," *Opt. Lett.* **25**(5), 320–322 (2000).
41. V. Ajeti et al., "Structural changes in mixed Col I/Col V collagen gels probed by SHG microscopy: implications for probing stromal alterations in human breast cancer," *Biomed. Opt. Express* **2**(8), 2307–2316 (2011).
42. P. P. Provenzano et al., "Collagen reorganization at the tumor-stromal interface facilitates local invasion," *BMC Med.* **4**(1), 38 (2006).
43. O. Nadiarnykh et al., "Alterations of the extracellular matrix in ovarian cancer studied by second harmonic generation imaging microscopy," *BMC Cancer* **10**(94) (2010).
44. R. Lacomb, O. Nadiarnykh, and P. J. Campagnola, "Quantitative second harmonic generation imaging of the diseased state osteogenesis imperfecta: experiment and simulation," *Biophys. J.* **94**(11), 4504–4514 (2008).
45. M. Strupler et al., "Second harmonic imaging and scoring of collagen in fibrotic tissues," *Opt. Express* **15**(7), 4054–4065 (2007).
46. M. C. Oh, W. Y. Hwang, and J. J. Kim, "Integrated-optic polarization controlling devices using electro-optic polymers," *Etri. J.* **18**(4), 287–299 (1997).
47. H. Eklund, A. Roos, and S. T. Eng, "Rotation of laser-beam polarization in acoustooptic devices," *Opt. Quant. Electron.* **7**(2), 73–79 (1975).
48. S. Plotnikov et al., "Optical clearing for improved contrast in second harmonic generation imaging of skeletal muscle," *Biophys. J.* **90**(1), 328–339 (2006).
49. J. C. Mansfield et al., "Collagen fiber arrangement in normal and diseased cartilage studied by polarization sensitive nonlinear microscopy," *J. Biomed. Opt.* **13**(4), 044020 (2008).
50. V. Nucciotti et al., "Probing myosin structural conformation *in vivo* by second-harmonic generation microscopy," *Proc. Natl. Acad. Sci. USA* **107**(17), 7763–7768 (2010).
51. D. Rouede et al., "Modeling of supramolecular centrosymmetry effect on sarcomeric SHG intensity pattern of skeletal muscles," *Biophys. J.* **101**(2), 494–503 (2011).
52. E. A. Gibson et al., "Multiphoton microscopy for ophthalmic imaging," *J. Ophthalmol.* **2011**, 870879 (2011).
53. A. T. Yeh et al., "Selective corneal imaging using combined second-harmonic generation and two-photon excited fluorescence," *Opt. Lett.* **27**(23), 2082–2084 (2002).
54. S. V. Plotnikov et al., "Characterization of the myosin-based source for second-harmonic generation from muscle sarcomeres," *Biophys. J.* **90**(2), 693–703 (2006).
55. P. J. Su et al., "Discrimination of collagen in normal and pathological skin dermis through second-order susceptibility microscopy," *Opt. Express* **17**(13), 11161–11171 (2009).

56. R. W. Boyd, *Nonlinear Optics*, Academic Press, St Louis, Missouri (2003).
57. P. J. Su et al., "The discrimination of type I and type II collagen and the label-free imaging of engineered cartilage tissue," *Biomaterials* **31**(36), 9415–9421 (2010).
58. K. M. Hanson and C. J. Bardeen, "Application of nonlinear optical microscopy for imaging skin," *Photochem. Photobiol.* **85**(1), 33–44 (2009).
59. J. C. Mackenzi, "Ordered structure of stratum corneum of mammalian skin," *Nature* **222**(5196), 881–882 (1969).
60. S. J. Lin et al., "Discrimination of basal cell carcinoma from normal dermal stroma by quantitative multiphoton imaging," *Opt. Lett.* **31**(18), 2756–2758 (2006).
61. M. Roustit and J. L. Cracowski, "Non-invasive assessment of skin microvascular function in humans: an insight into methods," *Microcirculation* **19**(1), 47–64 (2012).
62. J. H. Lee et al., "Noninvasive *in vitro* and *in vivo* assessment of epidermal hyperkeratosis and dermal fibrosis in atopic dermatitis," *J. Biomed. Opt.* **14**(1), 014008 (2009).
63. B. R. Masters and P. T. C. So, "Confocal microscopy and multi-photon excitation microscopy of human skin *in vivo*," *Opt. Express* **8**(1), 2–10 (2001).
64. A. N. Bader et al., "Fast nonlinear spectral microscopy of *in vivo* human skin," *Biomed. Opt. Express* **2**(2), 365–373 (2011).
65. M. J. Koehler et al., "*In vivo* assessment of human skin aging by multiphoton laser scanning tomography," *Opt. Lett.* **31**(19), 2879–2881 (2006).
66. K. Konig et al., "Clinical optical coherence tomography combined with multiphoton tomography of patients with skin diseases," *J. Biophotonics* **2**(6–7), 389–397 (2009).
67. S. J. Lin et al., "Discrimination of basal cell carcinoma from normal dermal stroma by quantitative multiphoton imaging," *Opt. Lett.* **31**(18), 2756–2758 (2006).
68. S. Psilodimitrakopoulos et al., "*In vivo*, pixel-resolution mapping of thick filaments' orientation in nonfibrilar muscle using polarization-sensitive second harmonic generation microscopy," *J. Biomed. Opt.* **14**(1), 014001 (2009).
69. S. Psilodimitrakopoulos et al., "Quantitative discrimination between endogenous SHG sources in mammalian tissue, based on their polarization response," *Opt. Express* **17**(12), 10168–10176 (2009).
70. R. Cicchi et al., "Scoring of collagen organization in healthy and diseased human dermis by multiphoton microscopy," *J. Biophotonics* **3**(1–2), 34–43 (2010).
71. I. Amat-Roldan et al., "Fast image analysis in polarization SHG microscopy.," *Opt. Express* **18**(16), 17209–17219 (2010).
72. D. A. Kleinman, "Nonlinear dielectric polarization in optical media," *Phys. Rev.* **126**(6), 1977–1978 (1962).
73. S. W. Chu et al., "Studies of $x((2))/x((3))$ tensors in submicron-scaled bio-tissues by polarization harmonics optical microscopy," *Biophys. J.* **86**(6), 3914–3922 (2004).
74. C. P. Pfeffer, B. R. Olsen, and F. Legare, "Second harmonic generation imaging of fascia within thick tissue block," *Opt. Express* **15**(12), 7296–7302 (2007).
75. A. M. Pena et al., "Chiroptical effects in the second harmonic signal of collagens I and IV," *J. Am. Chem. Soc.* **127**(29), 10314–10322 (2005).
76. P. J. Campagnola et al., "Three-dimensional high-resolution second-harmonic generation imaging of endogenous structural proteins in biological tissues," *Biophys. J.* **82**(1 Pt 1), 493–508 (2002).
77. F. Tiaho, G. Recher, and D. Rouede, "Estimation of helical angles of myosin and collagen by second harmonic generation imaging microscopy," *Opt. Express* **15**(19), 12286–12295 (2007).
78. M. Strupler et al., "Second harmonic imaging and scoring of collagen in fibrotic tissues," *Opt. Express* **15**(7), 4054–4065 (2007).
79. F. Tiaho, G. Recher, and D. Rouede, "Estimation of helical angles of myosin and collagen by second harmonic generation imaging microscopy," *Opt. Express* **15**(19), 12286–12295 (2007).
80. A. Deniset-Besseau et al., "Measurement of the second-order hyperpolarizability of the collagen triple helix and determination of its physical origin," *J. Phys. Chem. B* **113**(40), 13437–13445 (2009).
81. I. Rocha-Mendoza et al., "Sum frequency vibrational spectroscopy: the molecular origins of the optical second-order nonlinearity of collagen," *Biophys. J.* **93**(12), 4433–4444 (2007).
82. P. J. Su et al., "Determination of collagen nanostructure from second-order susceptibility tensor analysis," *Biophys. J.* **100**(8), 2053–2062 (2011).
83. G. Latour et al., "*In vivo* structural imaging of the cornea by polarization-resolved second harmonic microscopy," *Biomed. Opt. Express* **3**(1), 1–15 (2012).
84. C. S. Liao et al., "Decrimping: the first stage of collagen thermal denaturation unraveled by in situ second-harmonic-generation imaging," *Appl. Phys. Lett.* **98**(15), 153703 (2011).
85. Z. Y. Zhuo et al., "Second harmonic generation imaging—a new method for unraveling molecular information of starch," *J. Struct. Biol.* **171**(1), 88–94 (2010).
86. V. A. Hovhannisyan et al., "Spatial orientation mapping of fibers using polarization-sensitive second harmonic generation microscopy," *J. Biophotonics* (2012).
87. F. Legare, C. Pfeffer, and B. R. Olsen, "The role of backscattering in SHG tissue imaging," *Biophys. J.* **93**(4), 1312–1320 (2007).
88. J. Mertz and L. Moreaux, "Second-harmonic generation by focused excitation of inhomogeneously distributed scatterers," *Optic. Comm.* **196**(1–6), 325–330 (2001).
89. S. W. Chu et al., "Selective imaging in second-harmonic-generation microscopy with anisotropic radiation," *J. Biomed. Opt.* **14**(1), 010504 (2009).
90. I. S. Saidi, S. L. Jacques, and F. K. Tittel, "Mie and Rayleigh modeling of visible-light scattering in neonatal skin," *Appl. Opt.* **34**(31), 7410–7418 (1995).
91. I. Gusachenko, G. Latour, and M. C. Schanne-Klein, "Polarization-resolved second harmonic microscopy in anisotropic thick tissues," *Opt. Express* **18**(18), 19339–19352 (2010).
92. D. Ait-Belkacem et al., "Influence of birefringence on polarization resolved nonlinear microscopy and collagen SHG structural imaging," *Opt. Express* **18**(14), 14859–14870 (2010).
93. S. Tang et al., "Effect of pulse duration on two-photon excited fluorescence and second harmonic generation in nonlinear optical microscopy," *J. Biomed. Opt.* **11**(2), 020501 (2006).
94. P. Schon et al., "Polarization and phase pulse shaping applied to structural contrast in nonlinear microscopy imaging," *Phys. Rev. A* **81**(1), 013809 (2010).